Implications on clinical scenario of gold nanoparticle radiosensitization in regards to photon energy, nanoparticle size, concentration and location

2011 Phys. Med. Biol. 56 4631

(http://iopscience.iop.org/0031-9155/56/15/001)

Phys. Med. Biol. **56** (2011) 4631–4647 doi:10.1088/0031-9155/56/15/001

Implications on clinical scenario of gold nanoparticle radiosensitization in regards to photon energy, nanoparticle size, concentration and location

E Lechtman[1], N Chattopadhyay[2], Z Cai[2], S Mashouf[1], R Reilly[2] and J P Pignol[1,3,4]

[1] Department of Medical Biophysics, Sunnybrook Health Sciences Centre, 2075 Bayview Avenue, Toronto, Ontario M4N3M5, Canada
[2] Department of Pharmaceutical Sciences, Leslie Dan Faculty of Pharmacy, University of Toronto, 144 College St., Toronto, Ontario M5S 3M2, Canada
[3] Department of Radiation Oncology, Sunnybrook Odette Cancer Centre, 2075 Bayview Avenue, Toronto, Ontario M4N3M5, Canada

E-mail: Jean-Philippe.Pignol@sunnybrook.ca

Received 3 March 2011, in final form 15 June 2011
Published 6 July 2011
Online at stacks.iop.org/PMB/56/4631

Abstract

Gold nanoparticle (AuNP) radiosensitization represents a novel approach to enhance the effectiveness of ionizing radiation. Its efficiency varies widely with photon source energy and AuNP size, concentration, and intracellular localization. In this Monte Carlo study we explored the effects of those parameters to define the optimal clinical use of AuNPs. Photon sources included ^{103}Pd and ^{125}I brachytherapy seeds; ^{169}Yb, ^{192}Ir high dose rate sources, and external beam sources 300 kVp and 6 MV. AuNP sizes were 1.9, 5, 30, and 100 nm. We observed a 10^3 increase in the rate of photoelectric absorption using ^{125}I compared to 6 MV. For a ^{125}I source, to double the dose requires concentrations of 5.33–6.26 mg g^{-1} of Au or 7.10×10^4 30 nm AuNPs per tumor cell. For 6 MV, concentrations of 1560–1760 mg g^{-1} or 2.17×10^7 30 nm AuNPs per cell are needed, which is not clinically achievable. Examining the proportion of energy transferred to escaping particles or internally absorbed in the nanoparticle suggests two clinical strategies: the first uses photon energies below the k-edge and takes advantage of the extremely localized Auger cascade. It requires small AuNPs conjugated to tumor targeted moieties and nuclear localizing sequences. The second, using photon sources above the k-edge, requires a higher gold concentration in the tumor region. In this approach, energy deposited by photoelectrons is the main contribution to radiosensitization; AuNP size and cellular localization are less relevant.

(Some figures in this article are in colour only in the electronic version)

[4] Author to whom any correspondence should be addressed.

0031-9155/11/154631+17$33.00 Printed in the UK

1. Background

In recent years, gold nanoparticles (AuNPs) have been actively investigated as a novel high-Z radiosensitizing agent (Pignol *et al* 2006, Hainfeld *et al* 2004, Pradhan *et al* 2009). The premise of AuNP radiosensitization relies on gold's increased photoelectric absorption cross-section relative to tissue (Pradhan *et al* 2009, Hainfeld *et al* 2008). Upon irradiation, this increased photon absorption results in a highly conformal energy deposition around the AuNPs, caused by the localized spray of escaping photoelectric products (photoelectrons, Auger electrons, and characteristic x-rays) (Carter *et al* 2007, Foley *et al* 2005). The appeal of the AuNP is enhanced by the large number of atoms per particle (ranging from 250 for a 2 nm AuNP to 835 000 for a 30 nm AuNP), a surface well suited for conjugation to tumor targeting moieties (Qian *et al* 2008, Chattopadhyay *et al* 2010), and gold's general biocompatibility (Connor *et al* 2005). These features of AuNPs offer support to the notion that AuNP radiosensitization, as part of a future clinical strategy, might be both robust and tumor specific.

AuNP radiosensitization was first demonstrated *in vivo* by Hainfeld *et al* who showed a significant increase in long-term survival of mice bearing EMT-6 mammary carcinomas irradiated with 250 kVp photons after intravenous injection of non-targeted 1.9 nm AuNPs (Hainfeld *et al* 2004). Subsequently, AuNP radiosensitization has been observed in more controlled *in vitro* irradiation of cells and plasmid DNA (Foley *et al* 2005, Butterworth *et al* 2008, Brun *et al* 2009, Rahman *et al* 2009, Liu *et al* 2010). Butterworth *et al* showed single strand and double strand break enhancement of 2.29 and 1.25 respectively when irradiating plasmid DNA in the presence of 5 nm AuNPs (Butterworth *et al* 2008). Rahman *et al* observed a biological dose enhancement factor of up to 24.6 when irradiating bovine aortic endothelial cells with 80 kVp photons in the presence of 1.9 nm AuNPs (Rahman *et al* 2009).

While demonstrating the potential efficacy of AuNP radiosensitization, the large variations in these experimental results revealed AuNP radiosensitization to be highly sensitive to a number of physics and pharmacological parameters including irradiation energy and AuNP size, concentration, and intracellular localization (Hainfeld *et al* 2004, Butterworth *et al* 2008, Rahman *et al* 2009).

Toward understanding and predicting the effects of these parameters there have been a number of Monte Carlo simulation studies exploring AuNP dose enhancement at the macro, micro, and nano-scales (Carter *et al* 2007, Cho 2005, Cho *et al* 2009, Leung *et al* 2011, Zhang *et al* 2009, Zheng and Sanche 2009, Montenegro *et al* 2009, Jones *et al* 2010). Carter's simulation study showed that the dose deposited by the Auger cascade escaping a single nanoparticle fell below the background dose beyond a distance of 2 nm from the AuNP surface, suggesting that significant radiosensitization could only occur if nanoparticles are localized very close to the DNA inside the cell nucleus (Carter *et al* 2007). However, these findings seem to contradict *in vitro* data where significant radiosensitization has been noted for AuNPs localized far from the cell nucleus (Rahman *et al* 2009). On the other hand, Leung reported that photoelectrons and Auger electrons escaping AuNPs can travel distances as far as 3 μm to 1 mm from the AuNP, sufficient to reach the cell nucleus from endosomes, and even crossfire between cells (Leung *et al* 2011). Similar results were produced by Jones who examined various photon sources (^{125}I, ^{103}Pd, ^{169}Yb, ^{192}Ir, 50 kVp, and 6 MV x-rays), and simulated the dose distribution around clusters of gold inside cell endosomes. Jones observed a limited dose enhancement beyond distances of a few microns (Jones *et al* 2010).

The experimental and simulation studies published thus far have helped provide insight into the mechanism of radiosensitization, but they leave lingering questions as to which set of parameters define the optimal use of AuNPs for radiosensitization from a clinical paradigm. These clinical questions include: (1) How much gold, both in terms of the number of AuNPs per

cell and in mg of AuNPs per gram of the tumor, is required for a significant dose enhancement? (2) How does the photon source energy and AuNP size influence the spatial distribution of the energy deposited around AuNPs? (3) When is active cell/nucleus targeting of AuNPs most beneficial? In this Monte Carlo simulation study we explored the interplay of photon source energy, nanoparticle size, and intracellular location on AuNP radiosensitization in order to address these questions and to define the optimal use of AuNPs as radiosensitizers as part of a potential clinical strategy.

2. Materials and methods

2.1. Parameters investigated and metrics evaluated

The metrics studied here included the rate of photoelectric absorption in AuNPs of various sizes (1.9, 5, 30, and 100 nm diameter), the subsequent dose enhancement in the surrounding medium, and the energy and range of the escaping electron cascade. These metrics were expressed in terms of number of gold atoms, number of AuNPs, and also milligrams of AuNPs in order to comprehensively compare the effects of various AuNP sizes. The metrics were evaluated either per photoelectric absorption, or per 2 Gy prescribed dose to tumor in order to facilitate clinical evaluation.

Clinical photon sources were simulated in this investigation including two external beam sources—the Gulmay D3300 (Gulmay Ltd, Chertsey, UK) 300 kVp kilovoltage x-ray therapy unit (average energy $\approx$ 100 keV) and the Philips SL 20 6 MV (Philips, The Netherlands) accelerator unit (average energy $\approx$ 2 MeV) (O'Malley *et al* 2006, Pignol and Keller 2009, Keller *et al* 2008), two high dose rate brachytherapy sources—the ^{192}Ir microSelectron-HDR (Nucletron, Neenendaal, The Netherlands) (average energy $\approx$ 395 keV) and the ^{169}YbHDR 4140 (Implant Sciences Corporation) (average energy $\approx$ 93 keV) (Daskalov *et al* 1998, Taylor and Rogers 2008), and two low dose rate brachytherapy seed sources—the ^{125}I IsoAid ADVANTAGE model IAI-125 (IsoAid LLC., Port Richey, FL, USA) (average energy $\approx$ 28 keV) and the ^{103}Pd IsoAID ADVANTAGE (IsoAid LLC., Port Richey, FL, USA) (average energy $\approx$ 21 keV) (Solberg *et al* 2002, Sowards 2007).

2.2. Monte Carlo simulation

Monte Carlo transport codes employed in this study included MCNP-5 (Los Alamos National Laboratory) with the ENDF/B-VII cross-section library and PENELOPE 2008.1 (Barcelona, Catalonia) (X-5 Monte Carlo Team 2003, Salvat *et al* 2008). Both of these codes were used to take advantage of their respective strengths. Briefly, MCNP-5 contains powerful variance reduction methods that allow for efficient calculation of macroscopic tallies. However, MCNP-5 is of limited use in nano-scale transport as it has a default energy cutoff below 1 keV and uses a condensed history algorithm for the transport of electrons. PENELOPE on the other hand can simulate in a detailed way, the transport of electrons down to 50 eV, corresponding to electron ranges of about 2–4 nm (Cole 1969). PENELOPE was therefore used to simulate the production and transport of Auger cascades as they escaped the AuNPs after a photoelectric event, and to evaluate the subsequent dose deposited around AuNPs.

For a more illustrative depiction of AuNP radiosensitization, an in-house visualization tool was developed in Matlab (Natick, Massachusetts) to import the track histories from PENELOPE simulations and plot the paths of escaping particles around the AuNP in 3D. This was achieved by modifying the PENELOPE file PENMAIN.F, and recompiling the program. Flag variables were created to print the energy, position, and production information of all

particles escaping the AuNP after a photoelectric event. Escaping particles were followed event by event until termination due to the energy cutoff.

2.3. Simulation geometry and tallies

The first set of simulations evaluated the photon energy spectra after tissue penetration (ICRU four component soft tissue (National Institute of Standards and Technology 2010)), as well as the rate of photoelectric absorption in AuNPs within the tissue. These simulations were carried out using MCNP in photon mode. Photon showers were simulated penetrating a tissue depth of 1 and 5 cm for brachytherapy sources and external beam sources, respectively. Brachytherapy sources were described in detail including seed casings (Daskalov *et al* 1998, Taylor and Rogers 2008, Solberg *et al* 2002, Sowards 2007). The generation of the photon phase-space for the 6 MV and 300 kVp external beam sources has been described in detail in a previous publication (O'Malley *et al* 2006, Pignol and Keller 2009, Keller *et al* 2008). Due to the low probability of photons interacting with individual nanoparticles imbedded at a depth in tissue, AuNPs were not modeled in this simulation geometry. Rather a variance reduction approach using MCNP's FM function tally multiplier was utilized in the tally volume to predict the AuNP photoelectric absorption within this region. The FM function allows for the calculation of tallies in materials that are not present in the simulation volume and hence do not influence the particle transport. A 1 mm thick tally volume consisting of tissue was used to score the photon flux using the F4 tally. This flux tally was used to calculate the rate of photoelectric absorption in gold with the FM multiplier tally. The rate of photoelectric absorption was then normalized to the volume of a single AuNP and per 2 Gy prescribed dose to the tally volume using the *F8 tally function. $1 \times 10^9 - 2 \times 10^{10}$ source particles were simulated for each calculation maintaining a standard error of less than 0.1%.

The second set of simulations examined the characteristics of the photoelectric absorptions, the subsequent spray of the photoelectric products escaping AuNPs, and the dose enhancement in the surrounding tissue due to the enhanced photoelectric absorption in AuNPs. Detailed event-by-event MC simulations were performed in PENELOPE using the following parameters: EABS (1:3) = 50 50 50; C1 = 0; C2 = 0; WCC = 0; WCR = –100. The geometry consisted of a single AuNP (1.9, 5, 30 and 100 nm) embedded in a large volume of tissue (10 cm radius). Photons were initiated adjacent the AuNP directed toward it from a disk with radius equal to the AuNP radius. The input photon source energy spectra were obtained from the tissue-penetrated photon energy spectra collected from the first set of simulations. A customized main steering program in PENELOPE based on PENMAIN.F was developed to include unique tallies. These customized tallies measured the relative rate of absorption in each orbital of the gold atom, the number and energy of electrons escaping the AuNP per photoelectric absorption, the dose deposited to a 1 cm radius sphere of tissue surrounding the AuNP, and the distance traveled by Auger and photoelectrons in the surrounding tissue after escaping the AuNP. The distance or range was defined here as the maximum distance from the surface of the AuNP reached by each escaping electron. To reduce simulation time and to avoid following primary photons that did not interact with the AuNP, each PENELOPE simulation was split into two components. The first component included only the AuNP with no surrounding medium. A customized phase space file recorded the energy, position, and direction of the photoelectric products as they escaped the surface of the AuNP. Over 1×10^6 escaping particles were recorded for each simulation and the numbers of photoelectric absorptions were recorded for normalization. The second component of the simulation used this phase space file as the source input to follow the particles in the surrounding tissue volume. Tallies were normalized by the number of primary photoelectric absorptions. The dose was

Table 1. Number of photoelectric absorptions per AuNP per 2 Gy prescribed dose at a tissue depth of 1 and 5 cm for brachytherapy sources and external beam sources, respectively.

	Photon source (average energy)[a]					
AuNP diameter	Pd-103 (20.6 keV)	I-125 (27.0 keV)	Yb-169 (100.7 keV)	300 kVp (127.1 keV)	Ir-192 (324.3 keV)	6 MV (1861 keV)
1.9 nm	7.38×10^{-6}	6.47×10^{-6}	1.29×10^{-6}	7.62×10^{-7}	5.28×10^{-8}	6.43×10^{-9}
5 nm	1.34×10^{-4}	1.18×10^{-4}	2.34×10^{-5}	1.39×10^{-5}	9.61×10^{-7}	1.17×10^{-7}
30 nm	2.90×10^{-2}	2.55×10^{-2}	5.06×10^{-3}	3.00×10^{-3}	2.08×10^{-4}	2.53×10^{-5}
100 nm	1.08	9.43×10^{-1}	1.87×10^{-1}	1.11×10^{-1}	7.69×10^{-3}	9.38×10^{-4}
Per mg AuNP	1.06×10^{11}	9.33×10^{10}	1.85×10^{10}	1.10×10^{10}	7.61×10^{8}	9.28×10^{7}
Per Au atom	3.48×10^{-8}	3.05×10^{-8}	6.06×10^{-9}	3.60×10^{-9}	2.49×10^{-10}	3.04×10^{-11}

[a]Average photon energy at tissue depth of 1 and 5 cm for brachytherapy sources and external beam sources, respectively.

further normalized to a 2 Gy prescribed dose to the tissue (using the rate of photoelectric absorption in the AuNP per 2 Gy from the MCNP simulation results). The dose enhancement per AuNP was finally expressed both in terms of the number of AuNPs per cell (cell mass estimated at 3.37×10^{-12} kg), and the mg of AuNPs per gram of tumor required to double the prescribed dose to the tumor region. $7 \times 10^7 - 3 \times 10^{11}$ source particles were simulated for each configuration (depending on both the AuNP size and photon source energy) maintaining an average uncertainty of less than 1% for all tallies.

3. Results

3.1. Rate of photoelectric absorption

Results from the first MC simulation reveal a large increase in photoelectric absorption in the AuNPs for the lower energy sources and larger AuNP diameters (table 1). Specifically, the number of 30 nm AuNPs required to generate a single photoelectric event per cell with the 6 MV source was about 39 500 AuNPs, corresponding to 3.29×10^{10} Au atoms. In contrast, the number of 30 nm AuNPs required for a single photoelectric absorption with the ^{125}I source was about 39 AuNPs, corresponding to 3.28×10^7 Au atoms. This represents an increase in photoelectric absorption by three orders of magnitude. The rate of photoelectric absorption as a function of AuNP size simply follows a radius-cubed relation, and therefore nearly a four orders of magnitude increase in photoelectric absorption was observed between 5 and 100 nm AuNP.

Comparing the relative rate of photoelectric absorption in each orbital provides insight into the resulting relaxation cascade, and therefore the resulting energy and range of the photoelectric products released from such absorptions. These results, normalized per photoelectric absorption are summarized in table 2. At energies below the k-edge of gold (80.7 keV), photoelectric absorption can only occur through outer atomic shells (e.g. L,M,N). With the 300 kVp source, the ^{192}Ir source, and the 6 MV source we observed a significant absorption in the K-shell. These inner-shell absorptions transfer more energy into the surrounding medium compared to an outer-shell absorption. So while there is a higher overall rate of photoelectric absorption from lower energy sources, the energy released per absorption increases with increasing photon source energy.

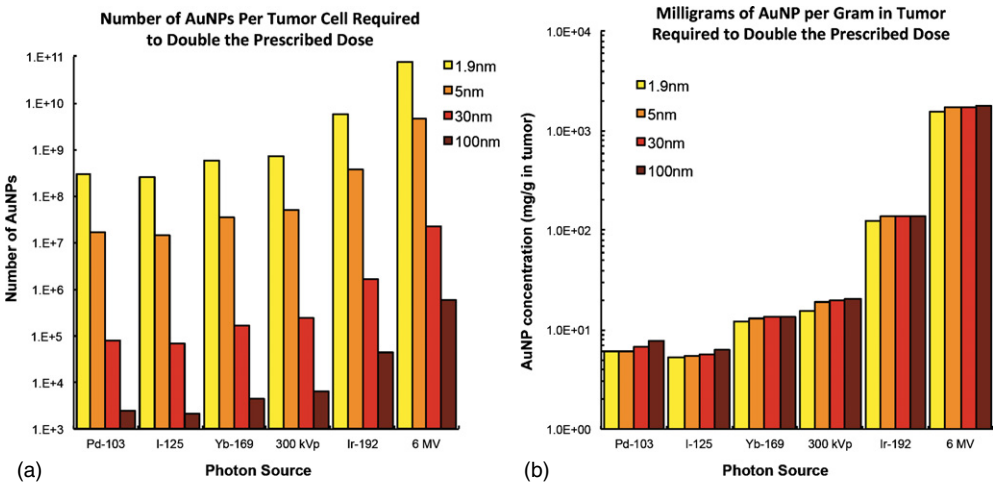

Figure 1. Simulation results of amount of AuNPs required to double the prescribed dose to the tumor as a function of different clinical photon sources and AuNP size, expressed as both the number of AuNPs per tumor cell (a) and milligrams of AuNPs per gram of tumor (b).

Table 2. Relative rate of photoelectric absorption (in%) in the atomic orbitals of gold per photoelectric event.

	Photon source (average energy of absorbed photon)					
Orbital	Pd-103 (20.48 keV)	I-125 (26.07 keV)	Yb-169 (62.11 keV)	300 kVp (97.85 keV)	Ir-192 (157.0 keV)	6 MV (99.85 keV)
K	–	–	13.22	56.69	52.97	30.25
L1	17.95	21.18	26.73	15.23	16.69	14.83
L2	24.32	23.82	18.51	8.64	8.89	12.87
L3	33.86	31.35	21.37	9.37	9.68	18.27
M1	4.40	5.00	6.03	3.36	3.83	4.23
M2	4.27	4.39	3.77	1.81	2.02	3.51
M3	6.25	6.10	4.58	2.09	2.32	5.17
M4	1.67	1.30	0.60	0.23	0.41	2.31
M5	2.02	1.59	0.66	0.26	0.49	3.01
Outer shells	5.26	5.29	4.53	2.31	2.69	5.55

3.2. Dose enhancement

Results from the second set of simulations exploring dose enhancement reveal a general trend of increasing dose enhancement using lower energy sources (figure 1). However, as the source energy becomes too low (as with ^{103}Pd) this trend breaks down.

Figure 1 expresses the amount of AuNPs required to double the prescribed dose to the tumor both in terms of number of AuNPs per tumor cell (figure 1(a)), and in terms of milligrams of AuNPs per gram of tumor (figure 1(b)). Examining the number of AuNPs per cell required to double the prescribed dose, in the worst-case scenario, with a 6 MV source and 1.9 nm AuNPs, one would require 7.59×10^{10} AuNPs per cell. In the most efficient scenario, with a ^{125}I seed source and 100 nm AuNPs, only 1.83×10^{3} AuNPs per cell would be needed to double the dose. Examining the results in terms of AuNP mass concentration, the worst-case

scenario would use the 6 MV source and 100 nm AuNPs, and would require 1760 mg of AuNPs per gram of tumor. This concentration would be clinically infeasible to accomplish. The most efficient scenario, using a ^{125}I brachytherapy source and 1.9 nm AuNPs, would require 5.33 mg AuNP per gram of tumor. Dose enhancement as a function of AuNP size was not observed to be strictly proportional to the AuNP radius-cubed. This can be attributed to low-energy Auger and delta electrons being absorbed more readily within AuNP of increasing size.

3.3. Photoelectric energy conversion

Figure 2 summarizes the percentage of energy from an absorbed photon transferred to escaping Auger and delta electrons, photoelectrons, characteristic x-rays, or internally absorbed within the nanoparticle. As the AuNP size is increased, energy from Auger and delta electrons is increasingly internally absorbed in the AuNP. Conversely, the percentage of energy escaping as photoelectrons and characteristic x-rays remains mostly unchanged for the AuNP sizes investigated in this study. As the primary photon energy is increased, the percentage of escaping energy from photoelectrons and characteristic x-rays increases due to K-shell ionizations. Figure 3 shows the photon energy spectrum escaping a 30 nm AuNP from the 300 kVp source and the ^{103}Pd source illustrating the contribution of K-shell ionizations. Understanding how the energy is distributed after a photoelectric absorption also sheds light on the spatial distribution of the energy that leaves the AuNPs. Auger and delta electrons have a very short range (less than 1 μm), photoelectrons can travel much further (up to hundreds of microns) and characteristic x-rays can travel as far as centimeters.

3.4. Characteristics of escaping electrons

Figure 4 depicts the range of escaping electrons. These plots consist of logarithmically spaced bins normalized per photoelectric event and to the bin width. It can be observed that each curve contains at least two distinct relative peaks—the first located around 0.02–0.1 μm and the second around 0.25–1.5 μm corresponding to electron energies of approximately 0.8–2.5 and 4.5–12 keV, respectively. These electron energies correspond to Auger electrons emitted from non-radiative transitions from shells L and M. Another subtle relative peak can be observed for the 1.9 nm AuNP for all energies, located around 0.004–0.01 μm corresponding to energies of 60–200 eV. While this demonstrates the release of very low electrons from the 1.9 nm AuNP, the precise interpretation of this peak is likely confounded by the inherent uncertainty of low-energy Monte Carlo simulation (Salvat *et al* 2008). Other unique humps on certain range spectrums can be traced back to relative peaks in their respective incoming photon spectrums.

As a function of AuNP size, one can observe the effects of internal absorption with larger AuNP sizes. The range plots depict more electrons with very short ranges for smaller AuNPs, due to the fact that low-energy electrons are able to escape the AuNP. Specifically, about 2.6 low-energy Auger and delta electrons escape per photoelectric event from the 1.9 nm AuNP, while less than 1 Auger and delta electron was observed to escape for the 100 nm AuNP. This result was similar for all photon energies investigated.

Figure 5 displays the electron ranges for a 30 nm AuNP for all photon sources in relation to the size of a hypothetical 10 μm cell radius indicated by a vertical marker. Another vertical marker represents the maximum range of escaping Auger and delta electrons. The maximum range was defined here as the range beyond which there is a 95% probability that any 1 Auger or delta electron will not exceed. This plot offers insight into the magnitude of 'cross-firing' that can be expected if AuNPs accumulate in some cells but not in others. For lower energy

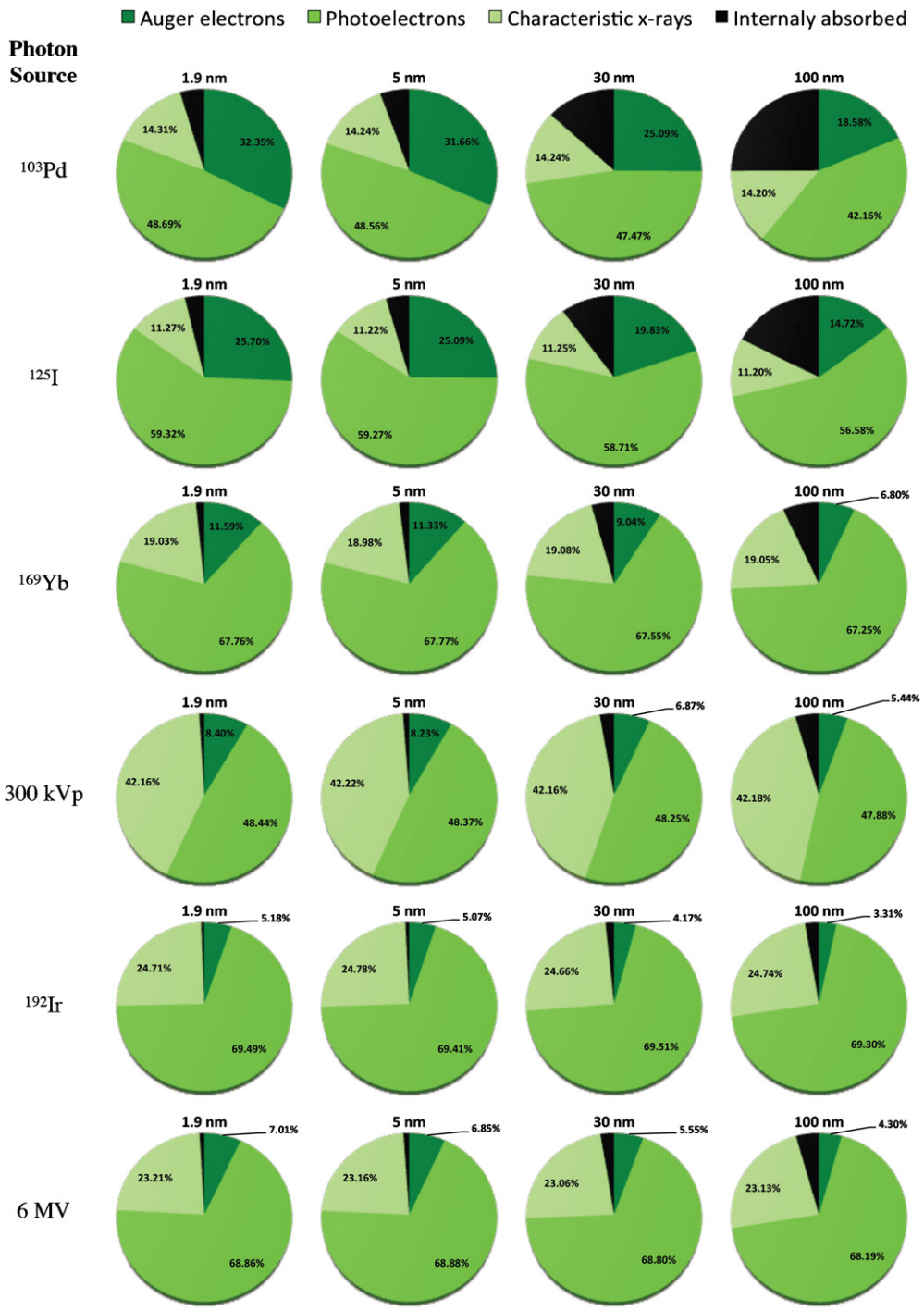

Figure 2. Pie charts representing the percentage of energy converted into escaping particles or internally absorbed per photoelectric absorption in a AuNP.

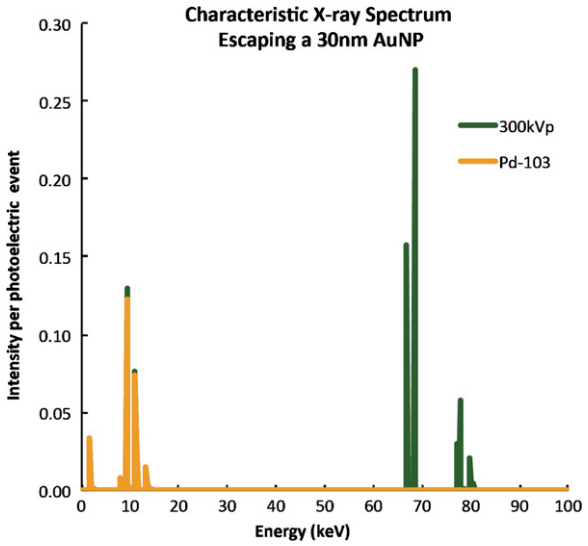

Figure 3. Characteristic x-ray spectrum escaping a 30 nm AuNP from the 300 kVp source and the ^{103}Pd source, illustrating the contribution of K-shell ionizations.

sources such as ^{103}Pd and ^{125}I, most electron ranges are confined to a single cell, while for higher source energies, photoelectrons can cross-fire between cells. Figure 6 provides a 3D visualization of the typical difference in distance traveled by the escaping electrons from a low-energy source and a high-energy source. This figure also includes the tracking of electrons liberated in the surrounding water from electrons that originated in the AuNP.

Table 3 presents the mean energy divided by the mean range of the escaping electrons. This quantity provides some insight into the relative biological effectiveness of the escaping electrons. The trend demonstrates that lower energy electrons deposit their energy within proportionally shorter ranges than higher energy electrons.

4. Discussion

The results presented in this study provide clinically relevant insight as to the effects of photon source energy and AuNP size on the rate of photoelectric absorption and the subsequent spatial distribution of secondary radiation emitted from the AuNPs. Compared to previously published work, our simulations explored AuNP radiosensitization in clinically relevant configurations including the simulation of primary photon tissue penetration, results normalized to 2 Gy prescribed dose, and concentration of gold expressed in terms of number of AuNPs per cancer cell, number Au atoms per cell, and mg of AuNPs per gram of tumor. We have also uniquely explored in detail the percentage of energy converted to Auger and delta electrons, photoelectrons, characteristic x-rays, or internally absorbed in AuNPs per photoelectric event. Our results offer further support of a pronounced AuNP radiosensitization effect in conjunction with photon energies below the k-edge of gold, as was shown in previous publications by Brun *et al* (2009), Cho *et al* (2009), Leung *et al* (2011), Montenegro *et al* (2009), Jones *et al* (2010). The pronounced dose enhancement for energies below the k-edge (figure 1) can be explained by the increased photoelectric absorption associated with lower energy sources (table 1). However, we will also discuss the potential clinical use of AuNPs in conjunction with energies above the k-edge.

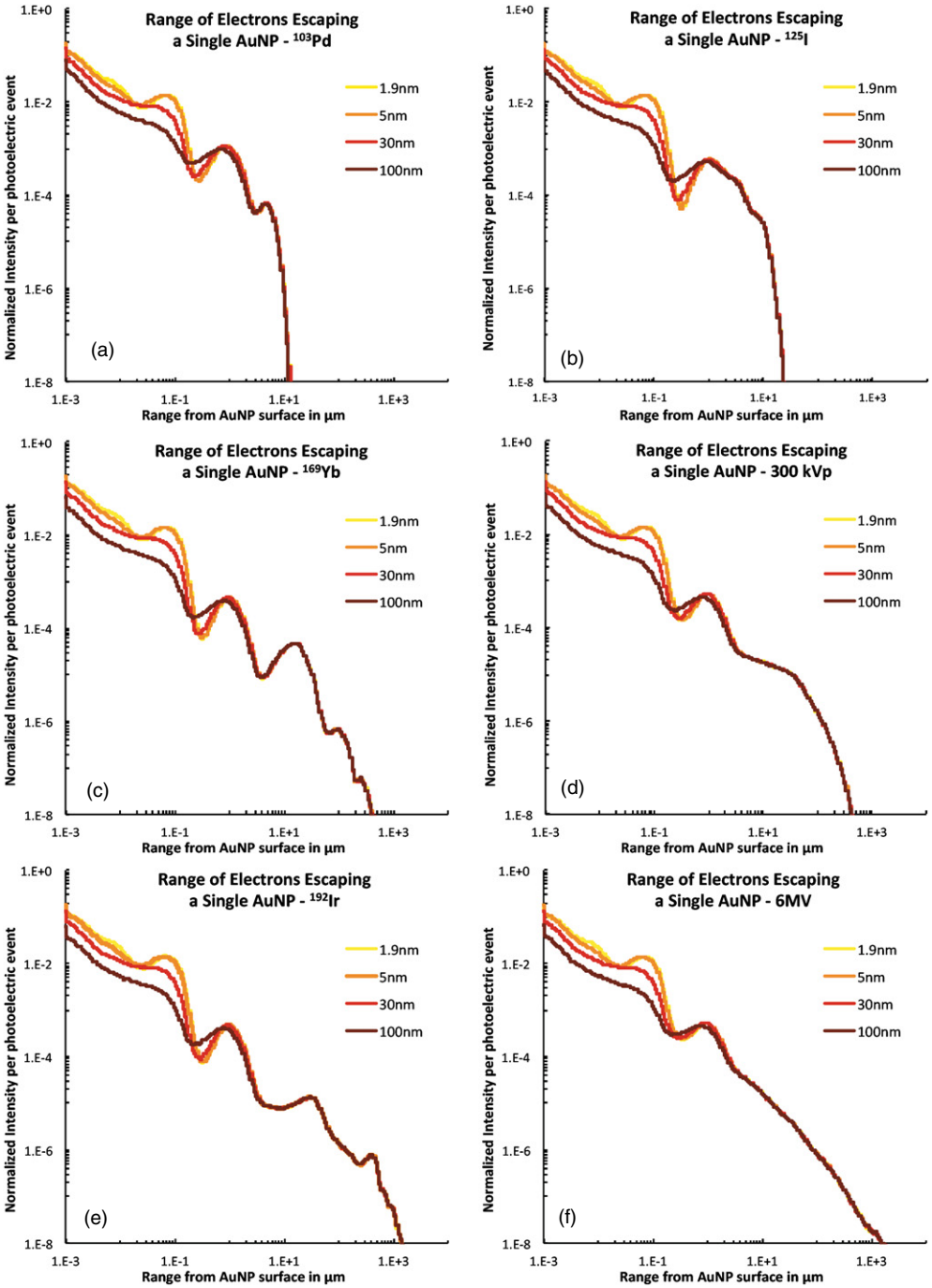

Figure 4. The range of escaping electrons from each photon source as a function of AuNP size. Range curves consist of logarithmically spaced bins normalized per photoelectric event and to the bin width.

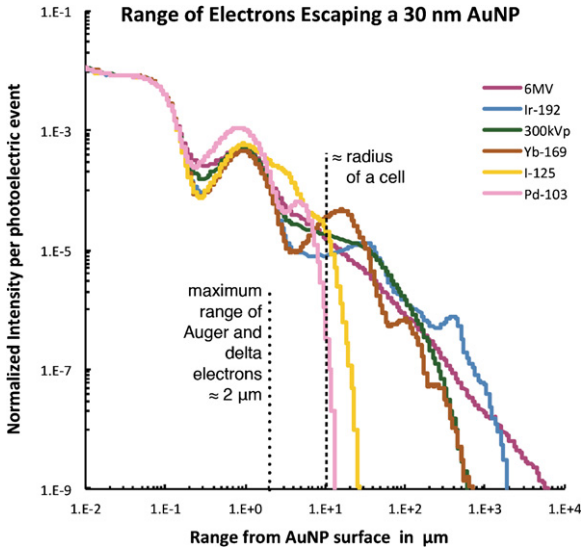

Figure 5. The range of electron escaping a 30 nm AuNP from each photon source relative to the dimensions of a cell.

Table 3. Ratio of mean energy over mean range of escaping electrons (keV μm^{-1}).

	Photon source							
	Pd-103				I-125			
AuNP diameter (nm)	1.9	5	30	100	1.9	5	30	100
Auger and delta electrons	8.54	8.46	7.73	7.50	8.56	8.50	7.74	7.48
Photoelectrons	4.77	4.78	4.82	4.82	3.62	3.62	3.64	3.70
All electrons	7.47	7.39	6.61	6.16	7.18	7.10	6.16	5.50
	Yb-169				300 kVp			
AuNP diameter (nm)	1.9	5	30	100	1.9	5	30	100
Auger and delta electrons	7.00	6.89	6.10	5.61	4.63	4.58	4.02	3.56
Photoelectrons	1.55	1.55	1.55	1.55	1.23	1.23	1.23	1.23
All electrons	5.52	5.39	4.38	3.50	3.69	3.63	2.98	2.38
	Ir-192				6 MV			
AuNP diameter (nm)	1.9	5	30	100	1.9	5	30	100
Auger and delta electrons	4.74	4.67	4.13	3.63	5.60	5.56	4.85	4.28
Photoelectrons	0.67	0.67	0.67	0.67	0.50	0.49	0.49	0.49
All electrons	3.61	3.54	2.81	2.10	4.12	4.07	3.18	2.35

(1) How much gold, both in terms of the number of AuNPs per cell and the mg of AuNPs per gram of the tumor, is required for a significant dose enhancement?

Our results indicate that to achieve a doubling of the prescribed dose in a tumor, the amount AuNPs required would need to be approximately 300 times greater for the 6 MV source compared to the lower energy brachytherapy sources. We therefore conclude that

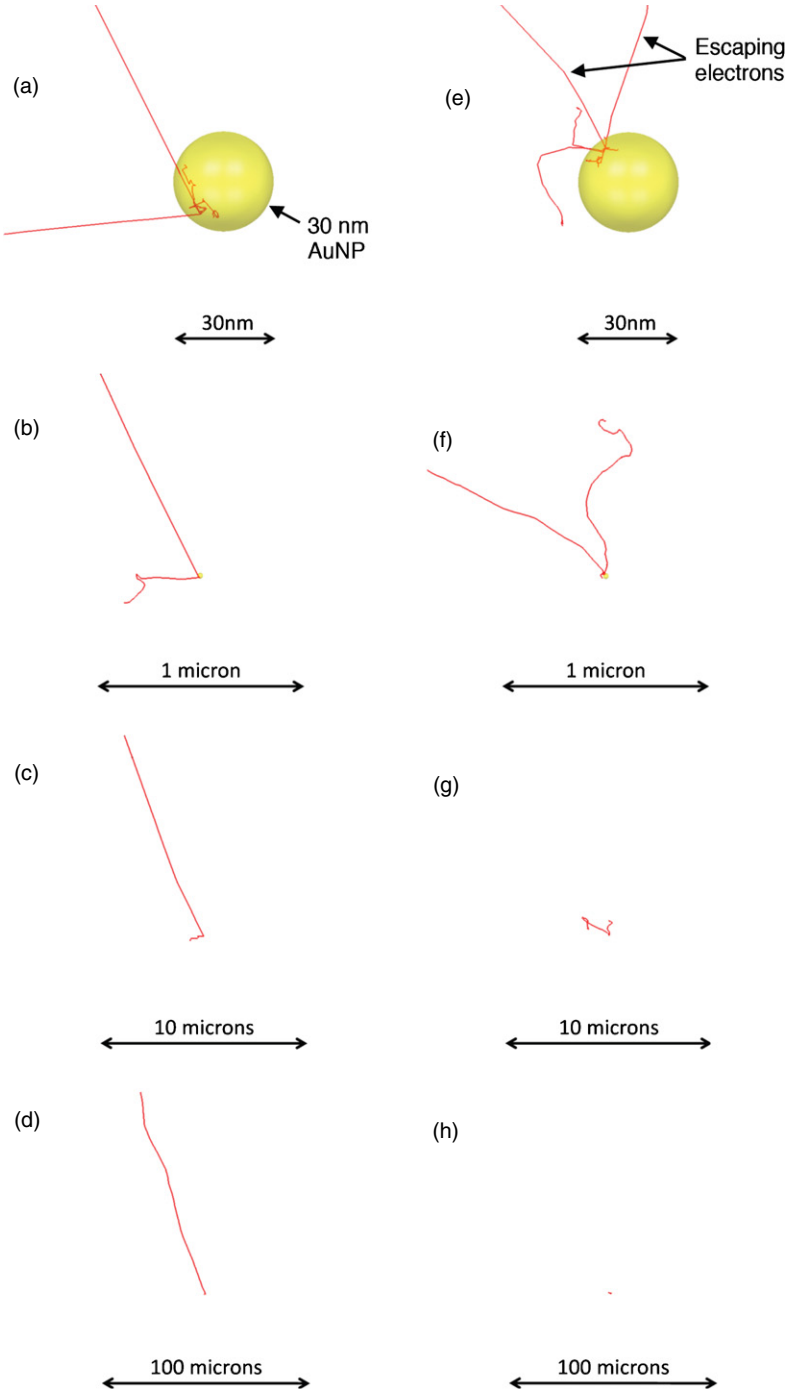

Figure 6. A zoom-out visualization of the photoelectric products produced from a single random photoelectric absorption in a single 30 nm AuNP. Electrons are represented in red. (a)–(d) The cascade of photoelectric products from a 6 MV source. (e)–(h) The cascade of photoelectric products from an I-125 source. These image sequences zoom out from the nano-scale (a) and (e) to 100 μm (d) and (h), contrasting the relative distance traveled by the escaping electrons from a low-energy source and a high-energy source.

AuNP radiosensitization using a 6 MV photon source is not clinically feasible. These results of dose enhancement are comparable to the findings of Cho's 2009 Monte Carlo study, as well as other theoretical estimates (Cho *et al* 2009, Roeske *et al* 2007). We have shown that in terms of the number of AuNPs per cell, larger particles produce significantly more dose enhancement than smaller particles due to the increased number of Au atoms. However, in terms of mg of AuNPs per gram of the tumor, smaller particles produce a greater dose enhancement allowing more low-energy electrons to escape into the surrounding tissue. Both metrics—the number of AuNPs per cell, and the mg of AuNPs per gram of tumor are useful in assessing AuNP radiosensitization from a clinical paradigm.

Previously published AuNP dosimetry papers have revealed the difficulty in applying the metric of dose to AuNP radiosensitization (Carter *et al* 2007, Cho 2005, Cho *et al* 2009, Leung *et al* 2011, Zhang *et al* 2009, Jones *et al* 2010). This is because the Auger cascades create uniquely localized dose heterogeneities at the nano-scale, depositing clusters of energy along the tracks of Auger electrons. The traditional concept of dose alone cannot properly treat the important spatial component of this energy distribution. A number of authors have examined the radial dose enhancement around AuNPs by defining concentric spheres to tally dose (Carter *et al* 2007, Leung *et al* 2011, Jones *et al* 2010). One issue with this approach may be the variation in scale associated with the increasingly large concentric volumes further away from the AuNP. While escaping electrons may travel many microns as we have shown, their contribution to the radial dose profile is not represented. These longer ranged electrons may still be effective in inducing biological lesions including single and double DNA strand breaks, especially toward the end of their track. In this study we have therefore purposely avoided simulating radial dose enhancement, and instead focused on electron range as a metric of the spatial energy distribution.

(2) How does the photon source and AuNP size influence the spatial distribution of the energy deposited around AuNPs?

Looking more carefully at the energy distribution in the surrounding medium from AuNP radiosensitization three distinct spatial zones can be identified. The first zone, comprising about 3–32% of the total escaping energy (depending on the AuNP size and photon source), and extending about 2 μm from the AuNP surface, is due to escaping Auger and delta electrons. The energy deposited in this zone has an increased relative biological effect due to the high linear energy transfer of these particles. Larger AuNP sizes tend to internally absorb these low-energy electrons and therefore reduce the relative energy contribution in this zone. The second zone, comprising about 42–69% of the total escaping energy, and extending up to hundreds of microns or beyond from the AuNP surface, is due to photoelectrons. These electrons lose their energy over a larger distance and can cross fire between cells, but can still cause significant DNA damage at the ends of their tracks. The contribution of these electrons depends mostly on the incoming photon spectrum, with more energetic photon sources producing higher energy and longer ranged photoelectrons. The third zone, comprising about 11–42% of the total escaping energy comes from escaping photons that can travel much larger distances from the AuNP. The conversion of an incoming photon into a characteristic x-ray will generally not significantly change its relative biological effect, and therefore this type of escaping energy may not contribute to AuNP radiosensitization.

Comparing our results of electrons ranges with those of Leung *et al* (2011), there are some similarities, but also a large discrepancy especially for the 6 MV source. For example, the average range of electrons escaping a 100 nm AuNP using a 6 MV source was 1090 μm as reported by Leung, whereas we found this range to be 81 μm. This difference can be attributed

to the fact that our simulations did not include Compton interactions within AuNPs, whereas Leung's study did include Compton interactions. We decided to exclude Compton interactions because AuNP radiosensitization results from gold's increased photoelectric absorption, and gold does not exhibit an enhanced Compton cross-section compared to tissue. Leung's electron range results using a 6 MV source therefore reflect the large distances traveled by Compton electrons set in to motion by high-energy photons. For lower energies, where Compton interactions are less frequent, our results are in better agreement with those of Leung.

(3) When is active cell/nucleus targeting of AuNPs most beneficial?

Our results reveal that as the photon source energy is reduced below the k-edge, AuNP localization becomes an increasingly important parameter. With the permanent seed sources, ^{103}Pd or ^{125}I, electrons escaping the AuNPs travel on the order of a micron on average, suggesting that AuNP cell internalization may be necessary for these Auger cascades to reach the DNA targets. Furthermore, to make use of the increased number of escaping Auger electrons as AuNP size is decreased, the AuNPs would need to be sufficiently close to the DNA. On the other hand for higher energy photon sources, where photoelectrons account for most of the escaping energy and significant cross firing occurs, AuNPs may not need to be precisely localized in the tumor cells to have a radiosensitizing effect.

With these results in mind, we can outline two potential clinical approaches employing AuNPs as radiosensitizers. The first potential approach involves clinical photon source energies below the k-edge where photoelectric absorption is most efficient. In this approach, a large number of small AuNPs must be accumulated in tumor cells, and localized within 2 μm of the cell nucleus to exploit the low-energy escaping Auger and delta electrons. AuNPs would therefore need to be conjugated to tumor specific cell surface markers and possibly nuclear localizing sequences (Mukherjee *et al* 2005, Nativo *et al* 2008, Sokolov *et al* 2003, Ryan *et al* 2007, Chen *et al* 2008). Small AuNPs are required here to avoid internal absorption of the low-energy Auger cascade, and for possible infiltration through the nuclear pore, which can allow translocation of particles as large as 30 nm (Tkachenko *et al* 2004). While the macroscopic dose enhancement with this strategy may not be profound, due to the difficulty of accumulating a very large number of individually targeted particles in the nucleus, smaller AuNPs release proportionally more low-energy Auger electrons in the immediate vicinity of the AuNPs. These Auger electrons are characterized by a higher linear energy transfer (LET). Increased LET has been shown to correlate well with an enhanced relative biological effectiveness up to LET values of about 100 keV μm^{-1} (Hall and Giaccia 2006). This radiosensitization approach can therefore be characterized by intense dose heterogeneities at the nano-scale. Thus, the number of AuNPs required per cell for a clinically significant effect using this approach may be significantly lower than we have predicted using a macroscopic dose metric. Taken as an upper limit, our results suggest that to achieve a doubling of the prescribed dose, 1.44×10^7 5 nm AuNPs would be required per cell (corresponding to 5.39 mg of AuNPs per gram of tumor).

In regards to the photon source energy, the clinical challenge with permanent brachytherapy seeds is that the prescribed dose is delivered continuously over the span of weeks. In this case it would be necessary to understand the full pharmacokinetic implications of different sized AuNPs with various conjugations to ensure they remain in the cancer cells for extended periods. With a half-life of 17 days, ^{103}Pd may be a more practical source than ^{125}I, which exhibits a half-life of 59.4 days. A more clinically relevant scenario could involve novel miniature electronic 50 kVp x-ray source in conjunction with a balloon catheter.

The second clinical strategy, involving higher energy photon sources above the k-edge such as the high dose rate ^{169}Yb source or the 300 kVp orthovoltage source, would constitute a bulk approach to AuNP radiosensitization. This strategy would exploit the more energetic photoelectrons escaping the AuNPs, which travel on the order of tens of microns and can easily reach the cell nucleus from outside the cell. AuNPs would not necessarily need to be internalized in the cancer cells because the relative distance from the DNA is not as crucial using higher energy sources. Accumulation could therefore be achieved passively by relying on the increased permeation and retention of the leaky vasculature of certain tumors. However, targeted AuNPs would still be beneficial in this case to ensure retention of nanoparticles in the tumor for the duration of the radiotherapy (Chattopadhyay *et al* 2010, Chithrani 2010). In this approach the size of AuNPs is less crucial as the main benefit of smaller particles is only realized at very small distances from the AuNPs.

Rather than recommending the number of AuNPs required per cell, a more fitting metric for this approach would be the mg of AuNPs per gram of tumor. Based on our calculations the concentration of AuNPs in the tumor region required to double the prescribed dose would be between 12.1–13.7 mg AuNP per gram for the ^{169}Yb HDR source and 15.4–20.2 mg AuNP per gram for the 300 kVP source. This approach requires significantly higher concentrations of AuNPs but does not necessitate the production of cellular or nuclear targeting AuNPs.

Acknowledgments

This research was supported by a grant from the Canadian Breast Cancer Research Alliance (CBCRA grant 019374) and by the Canadian Institute for Health Research (CIHR) Terry Fox Program—Ultrasound for Cancer Therapy from the Terry Fox Foundation. EL is the recipient of a Natural Sciences and Engineering Research Council of Canada (NSERC)—Alexander Graham Bell Scholarship. Niladri Chattopadhyay is supported by a Vanier Canada Graduate Scholarship from the Canadian Institute of Health Research, a pre-doctoral fellowship from the US Army Department of Defense Breast Cancer Research Program (W81XWH-08-1-0519, P00002), and a pre-doctoral fellowship from the Connaught Fund, University of Toronto. The authors thank Professor Francesc Selvat from the Facultat de Fisica, University of Barcelone, for graciously providing the PENELOPE code.

References

Brun E, Sanche L and Sicard-Roselli C 2009 Parameters governing gold nanoparticle x-ray radiosensitization of DNA in solution *Colloids Surf.* B **72** 128–34

Butterworth K T, Wyer J A, Brennan-Fournet M, Latimer C J, Shah M B, Currell F J and Hirst D G 2008 Variation of strand break yield for plasmid DNA irradiated with high-Z metal nanoparticles *Radiat. Res.* **170** 381–7

Carter J D, Cheng N N, Qu Y, Suarez G D and Guo T 2007 Nanoscale energy deposition by x-ray absorbing nanostructures *J. Phys. Chem.* B **111** 11622–5

Chattopadhyay N, Cai Z, Pignol J P, Keller B, Lechtman E, Bendayan R and Reilly R M 2010 Design and characterization of HER-2-targeted gold nanoparticles for enhanced x-radiation treatment of locally advanced breast cancer (LABC) *Mol. Pharm.* **7** 2194–206

Chen P C, Mwakwari S C and Oyelere A K 2008 Gold nanoparticles: from nanomedicine to nanosensing *Nanotechnol., Sci. Appl.* **1** 45–66

Chithrani D B 2010 Intracellular uptake, transport, and processing of gold nanostructures *Mol. Membr. Biol.* **27** 299–311

Cho S H 2005 Estimation of tumor dose enhancement due to gold nanoparticles during typical radiation treatments *Phys. Med. Biol.* **50** N163–73

Cho S H, Jones B L and Krishnan S 2009 The dosimetric feasibility of GNRT *Phys. Med. Biol.* **54** 4889–905

Cole A 1969 Absorption of 20-eV to 50 000-eV electron beams in air and plastic *Radiat. Res.* **38** 7–33

Connor E E, Mwamuka J, Gole A, Murphy C J and Wyatt M D 2005 Gold nanoparticles are taken up by human cells but do not cause acute cytotoxicity *Small* **1** 325–7

Daskalov G M, Löffler E and Williamson J F 1998 Monte Carlo-aided dosimetry of a new high dose-rate brachytherapy source *Med. Phys.* **25** 2200

Foley E A, Carter J D, Shan F and Guo T 2005 Enhanced relaxation of nanoparticle-bound supercoiled DNA in x-ray radiation *Chem. Commun.* **25** 3192–4

Hainfeld J F, Dilmanian F A, Slatkin D N and Smilowitz H M 2008 Radiotherapy enhancement with gold nanoparticles *J. Pharm. Pharmacol.* **60** 977–85

Hainfeld J F, Slatkin D N and Smilowitz H M 2004 The use of gold nanoparticles to enhance radiotherapy in mice *Phys. Med. Biol.* **49** N309–15

Hall E J and Giaccia A J 2006 *Radiobiology for the Radiologist* 6th edn (Philadelphia, PA: Lippincott Williams and Wilkins) pp 106–16

Jones B L, Krishnan S and Cho S H 2010 Estimation of microscopic dose enhancement factor around gold nanoparticles by Monte Carlo calculations *Med. Phys.* **37** 3809–16

Keller B M, Peressotti C and Pignol J P 2008 Optical imaging analysis of microscopic radiation dose gradients in Gafchromic EBT film using a digital microscope *Med. Phys.* **35** 3740–7

Leung M K K, Chow J C L, Chithrani B D, Lee M J G, Oms B and Jaffray D A 2011 Irradiation of gold nanoparticles by x-rays: Monte Carlo simulation of dose enhancements and the spatial properties of the secondary electrons production *Med. Phys.* **38** 1–8

Liu C J *et al* 2010 Enhancement of cell radiation sensitivity by pegylated gold nanoparticles *Phys. Med. Biol.* **55** 931–45

Montenegro M, Nahar S N, Pradhan A K and Huang K 2009 *J. Phys. Chem.* A **113** 12364–9

Mukherjee P, Bhattacharya R, Wang P, Wang L, Basu S, Nagy J A, Atala A, Mukhopadhyay D and Soker S 2005 Antiangiogenic properties of gold nanoparticles *Clin. Cancer Res.* **11** 3530–4

National Institute of Standards and Technology 2010 *Composition of TISSUE, SOFT (ICRU FOUR-COMPONENT)* http://physics.nist.gov/cgi-bin/Star/compos.pl?matno=262 (accessed 10 January 2010)

Nativo P, Prior I A and Brust M 2008 Uptake and intracellular fate of surface-modified gold nanoparticles *ACS Nano* **2** 1639–44

O'Malley L, Pignol J P, Beachey D J, Keller B M, Presutti J and Sharpe M 2006 Improvement of radiological penumbra using intermediate energy photons (IEP) for stereotactic radiosurgery *Phys. Med. Biol.* **51** 2537–48

Pignol J P and Keller B 2009 Electron and photon spread contributions to the radiological penumbra for small monoenergetic x-ray beam ($\leqslant$2 MeV) *J. Appl. Phys.* **105** 102011–5

Pignol J P, Keller B, Rakovitch E and Sankreacha R 2006 First report of a permanent breast seed implant (PBSI) as adjuvant radiation for early stage breast cancer *Int. J. Radiat. Oncol. Biol. Phys.* **64** 176–81

Pradhan A K, Nahar S N, Montenegro M, Yu Y, Zhang H L, Sur C, Mrozik M and Pitzer R M 2009 Resonant x-ray enhancement of the auger effect in high-*Z* atoms, molecules, and nanoparticles: potential biomedical applications *J. Phys. Chem.* A **113** 12356–63

Qian X, Peng X H, Ansari D O, Yin-Goen Q, Chen G Z, Shin D M, Yang L, Young A N, Wang M D and Nie S 2008 *In vivo* tumor targeting and spectroscopic detection with surface-enhanced Raman nanoparticle tags *Nat. Biotechnol.* **26** 83–90

Rahman W N, Bishara N, Ackerly T, He C F, Jackson P, Wong C, Davidson R and Geso M 2009 Enhancement of radiation effects by gold nanoparticles for superficial radiation therapy *Nanomedicine* **5** 136–42

Roeske J C, Nunez L, Hoggarth M, Labay E and Weichselbaum R R 2007 Characterization of the theorectical radiation dose enhancement from nanoparticles *Technol. Cancer Res. Treat.* **6** 395–401

Ryan J A, Overton K W, Speight M E, Oldenburg C N, Loo L N, Robarge W, Franzen S and Feldheim D L 2007 Cellular uptake of gold nanoparticles passivated with BSA-SV40 large T antigen conjugates *Anal. Chem.* **79** 9150–9

Salvat F, Fernández-Varea J M and Sempau J 2008 PENELOPE, a code system for Monte Carlo simulation of electron and photon transport (Facultat de Fisica (ECM), Universitat de Barcelona, Spain)

Sokolov K, Follen M, Aaron J, Pavlova I and Malpica A 2003 Real-time vital optical imaging of precancer using anti-epidermal growth factor receptor antibodies conjugated to gold nanoparticles *Cancer Res.* **63** 1999–2004

Solberg T D, DeMarco J J, Hugo G and Wallace R E 2002 Dosimetric parameters of three new solid core I-125 brachytherapy sources *J. Appl. Clin. Med. Phys.* **3** 119–34

Sowards K T 2007 Monte Carlo dosimetric characterization of the IsoAid ADVANTAGE 103Pd brachytherapy source *J. Appl. Clin. Med. Phys.* **8** 18–25

Taylor R E P and Rogers D W O 2008 EGSnrc Monte Carlo calculated dosimetry parameters for ^{192}Ir and ^{169}Yb brachytherapy sources *Med. Phys.* **35** 4933–44

Tkachenko A G, Xie H, Liu Y, Coleman D, Ryan J, Glomm W R, Shipton M K, Franzen S and Feldheim D L 2004 Cellular trajectories of peptide-modified gold particle complexes: comparison of nuclear localization signals and peptide transduction domains *Bioconjugate Chem.* **15** 482–90

X-5 Monte Carlo Team 2003 *MCNP—A General Monte Carlo N-Particle Transport Code, Version* (Los Alamos, NM: Los Alamos National Laboratory)

Zhang S X, Gao J, Buchholz T A, Wang Z, Salehpour M R, Drezek R A and Yu T K 2009 Quantifying tumor-selective radiation dose enhancements using gold nanoparticles: a Monte Carlo simulation study *Biomed. Microdevices* **11** 925–33

Zheng Y and Sanche L 2009 Gold nanoparticles enhance DNA damage induced by anti-cancer drugs and radiation *Radiat. Res.* **172** 114–9